Oriental Pharmacy and Experimental Medicine (2020) 20:645–661
https://doi.org/10.1007/s13596-019-00406-9

RESEARCH ARTICLE

Ligand-based virtual screening, consensus molecular docking, multi-target analysis and comprehensive ADMET profiling and MD stimulation to find out noteworthy tyrosine kinase inhibitor with better efficacy and accuracy

Arifur Rahman[1,2] · Nazmul Hasan Naheed[1] · Sabreena Chowdhury Raka[1,3] · Nazmul Qais[4] · A. Z. M. Ruhul Momen[1]

Received: 20 August 2019 / Accepted: 4 October 2019 / Published online: 4 December 2019

Abstract
Inhibition of BCR–ABL tyrosine kinase plays a crucial role in the management of chronic myelogenous leukemia (CML). The suppression of CML is getting harder because of a distinct pattern of resistance. Developing new types of ABL tyrosine kinase inhibitors along with ABL2, CSF1R, KIT, LCK, PDGFRA, and PDGFRB inhibitors is the main objective of this study that may overcome the drug resistance issue. The current study has been conducted using a kinase database containing 177,000 bioactive molecules, the top 135 molecules were selected with the best docking score and subjected to comprehensive ADMET profiling, multi-target analysis. Based on consensus molecular docking score (AutoDock, Chimera, Achilles, and Mcule), 22 molecules have been screened out which later undertaken for ADME/T profiling. After profiling of ADME/T data, selected molecules subjected to docking with multiple targets. Finally, molecular dynamics simulations had performed to screen the binding accuracy of the four lead molecules with ABL1. MD simulations of the desired complex (ABL1, ABL2, CSF1R, KIT, LCK, PDGFRA, and PDGFRB, among them ABL1 was the prime target) performed and found that PCID 10181160 and PCID 72724706 are the most promising inhibitors comparing to imatinib. These lead molecules are the potential CML inhibitors that could resolve the resistance pattern. Further chemical synthesis, wet lab analysis, and experimental validation deserve the utmost attention.

Keywords Chronic myelogenous leukemia · Imatinib · Consensus docking · ADMET · Multi-target analysis · Molecular dynamics simulation

Background

Chronic myeloid leukemia (CML) is a myeloproliferative disease characterized by the translocation of a section of human chromosome 9 which contains ABL kinase domain with specific breakpoint cluster region (BCR) on chromosome 22 (Faderl et al. 1999). The ABL1 gene on chromosome 9 and BCR gene on chromosome 22 together involved in the formation of BCR–ABL which is basically the active oncogene tyrosine kinase (TK) (Kang et al. 2016). BCR–ABL tyrosine kinase plays a crucial role in the development of CML (Jabbour and Kantarjian 2014). Thus, the inhibition of BCR–ABL is the best possible option for the management of CML.

Imatinib, a tyrosine kinase inhibitor, inhibits ATP binding site of BCR–ABL. It prevents tyrosine phosphorylation and downstream signaling (Shah et al. 2002). Additionally, the conformation of tyrosine kinase changes over time due to mutation and made completely inaccessible to imatinib (Mauro 2006; Shah et al. 2013; Le Coutre et al. 2008; Steinberg 2007). BCR–ABL escalation at the genomic level has been associated with imatinib and other

✉ Arifur Rahman
arifur@pharm.jnu.ac.bd; rahman.arifpharma@gmail.com

1 Computational Biology Research Lab, Department of Pharmacy, Jagannath University, Dhaka 1100, Bangladesh

2 FDCC Testing and Research Lab, Department of Pharmacy, Jagannath University, 9-10, Chittaranjan Ave, Dhaka 1100, Bangladesh

3 Department of Pharmacy, Faculty of Allied Health Sciences, Daffodil International University, Dhaka 1207, Bangladesh

4 Department of Clinical Pharmacy and Pharmacology, Faculty of Pharmacy, University of Dhaka, Dhaka 1000, Bangladesh

kinase inhibitors' failure (Eadie et al. 2018). This failure may overcome by targeting specific protein instead of BCR–ABL (Druker et al. 2001). The effects of imatinib on a number of tyrosine kinases depicted in Fig. 1 (Szklarczyk et al. 2015).

Proto-oncogene tyrosine-protein kinase (KIT), Abelson (ABL2), Colony-stimulating factor 1 receptor (CSF1R), Lymphocyte-specific protein tyrosine kinase (LCK), Platelet-derived growth factor receptors A (PDGFRA), Platelet-derived growth factor receptors B (PDGFRB) are the notable target of interests which are further divided into two categories. Receptor protein kinase including BCR–ABL, ABL2, KIT, a CSF1R kinase domain and Non-Receptor protein kinase including PDGFRA, PDGFRB, LCK kinase domain (Rask-Andersen et al. 2014). Imatinib exhibited increased activity toward ABL. However, activity against PDGFR, KIT, and LCK never performed before. Thus, screening new inhibitors by targeting all these proteins may reveal a new, wider possibility for the management of CML.

Biologically active molecules were screened out from kinase database and further subjected to molecular docking, ADMET profiling, and molecular dynamics simulation in search of new inhibitor that could provide better affinity than imatinib (Quintás-Cardama et al. 2007; Goldman and Melo 2003; Krieger and Vriend 2014).

Materials and method

Selection and preparation of proteins

Targeted proteins had carefully chosen from the stitch database and SwissTargetPrediction web server. Crystal structure of proteins were retrieved from PDB is ABL1, ABL2, CSF1R, KIT, LCK, PDGFRA, PDGFRB, and their corresponding PDB IDs are 4WA9, 3GVU, 2I1 M, 4U0I, 2PL0, 5K5X and 3MJG. Ligand and water molecules removed using pymol. Missing residues were corrected using MOE (Molecular Operating Environment) protein preparation wizard. The bound Zn^{2+} and Cl^{-} ions removed and bond orders were determined. Proteins preparation performed by adding polar hydrogens and Gasteiger charge using Auto Dock Tool 1.5.6.

Binding site prediction

MetaPocket 2.0 has been used to predict the top three binding cavities of ABL2, CSF1R, KIT, LCK, PDGFRA, and PDGFRB proteins (Huang 2009). The accuracy of predicting binding pockets enhanced by means of the LIGSITE. Z-score evaluated to select the top binding cavities. Desired bioactive molecules had docked with the first pocket of the protein. In order to validate the pockets of the protein

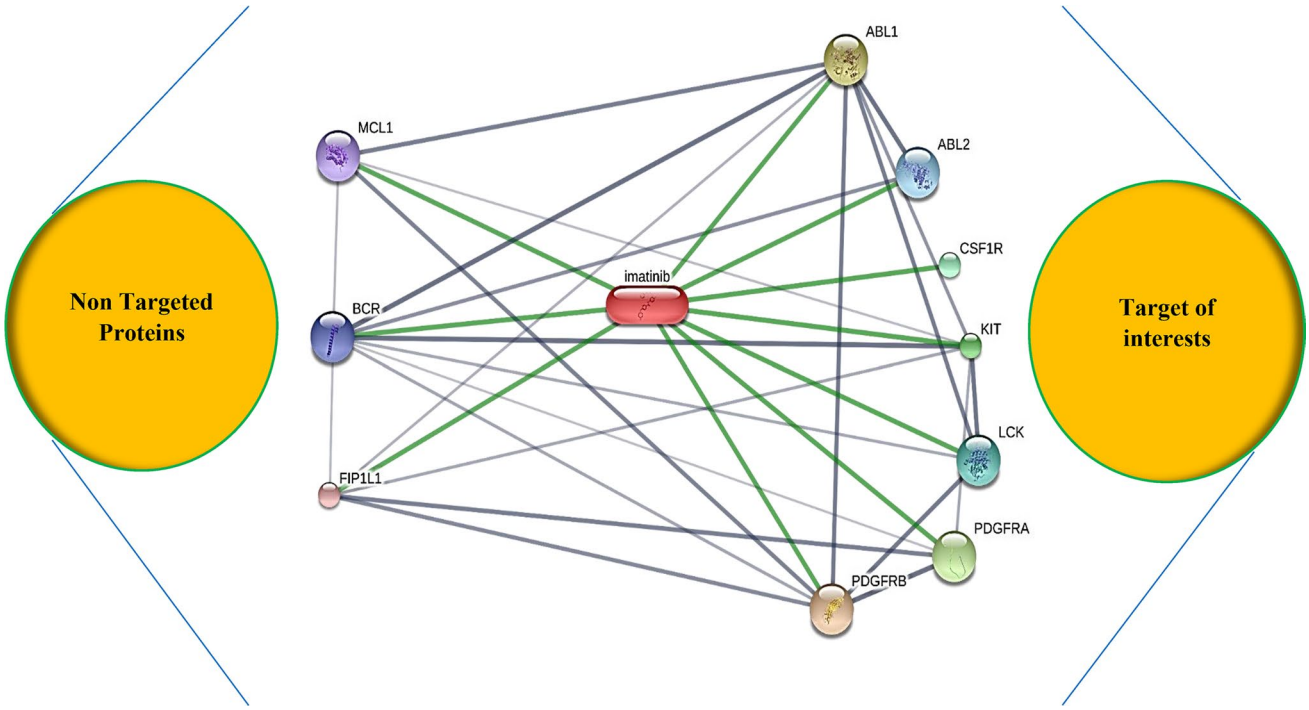

Fig. 1 Numerous targeted proteins for imatinib which were generated by STITCH server

obtained from MetaPocket, data compared with the CASTp server (Dundas et al. 2006).

Virtual screening and preparation of ligand molecules

Ligand-based virtual screening was carried out using a kinase database comprising 177,000 molecules (biological activity < 10 µM) and kinase inhibitor (ChEMBL) database. About 135 compounds were screened out which were closely similar to imatinib based on the cut-off value of above 80%. Selected structures downloaded from the PubChem database and prepared for docking studies. Polar hydrogen and Gasteiger charge added using Auto Dock Tool 1.5.6., and the energy of candidates minimized for docking purposes.

Molecular docking

135 bioactive molecules subjected for consensus docking studies using the AutoDock, Achilles, Mcule server (Morris et al. 1996; Nagasundaram et al. 2015; Pettersen et al. 2004; Hassan et al. 2017). The docking program calculated energies to obtain the best binding mode. Based on the binding energies better than Imatinib, 22 molecules had sorted out for further ADME/T profiling.

ADMET prediction

SwissADME, AdmetSAR, and DruLiTo tool were used to predict the topological polar surface area (TPSA), rotatable bonds, H-bond acceptors, H-bond donors, fraction Csp3 from physicochemical properties, iLOGP, WLOGP for lipophilicity, ESOL Class for solubility, Pharmacokinetics profile, Lipinski rule of 5, druglikeliness, AMES toxicity, carcinogenicity and acute oral toxicity. Finally, after ADME/T screening, four molecules passed all the criteria and selected as the top hits for molecular simulation study and multi-target analysis with ABL2, CSF1R, KIT, LCK, PDGFRA, and PDGFRB.

Molecular dynamics (MD) simulation of the complexes

ABL1 complexed with the top hits were subjected to MD simulation using YASARA in Windows 64-bit operating system (Krieger and Vriend 2015; Mitra and Dash 2018). Each complex cleaned and hydrogen bond network had optimized. Refinement of these complexes performed with subsequent relaxation by steepest descent minimization and subjected for full potential energy minimization for 5000 cycles until convergence reached. After that complexes were set for simulation annealing minimization to adapt with deleted water (Isa et al. 2018; Mandlik and Singh 2016; Jakalian et al. 2002; Pascoini et al. 2018). At constant pressure, MD simulation of these complexes had carried out for a period of 50 ns. Force field parameters for the complexes obtained by using the AMBER force field (Krieger et al. 2002, 2006; Dickson et al. 2014). The complexes had placed in a cubic box and filled with transferable intermolecular potential 3P (TIP3P) water molecules (Skelton et al. 2011). All simulations had performed at 298 K under certain periodic boundary conditions. The pH set to 7.4 and 0.9% NaCl had maintained. Time step had used with force cut-off 8 Å. Solvent density assigned for 0.997 g/ml. Each simulation system consisted of $29{,}400 \pm 140$ atoms. Using the YASARA structure built-in macros the resulting trajectories subjected to analyze the stability. To understand the relative stability of the ligand inside its binding pocket, hydrogen bonds between the solute and solvent analyzed. For further experimental validation, the radius of gyration (Rg) of the solute, RMSD and RMSF of the ligand bound protein had generated (Krieger and Vriend 2015; Krieger et al. 2002; Maier et al. 2015; Stewart 1990; Wang et al. 2004; Meng et al. 2011; Sánchez-Linares et al. 2012).

Result and discussion

Consensus docking of bioactive ligands

In this study, consensus docking had performed to find out the best scores possible from 135 bioactive molecules obtain from the PubChem database. Consensus binding energies of 22 molecules showed in Table 1 and Fig. 2.

Results of Lipinski's rule, and Veber filter demonstrated in Table 2A&B. These consensus-binding scores had compared with imatinib and presented in Fig. 3. 22 bioactive molecule and ABL1 protein residual interactions showed in Table 3.

ADMET analysis

The 22 compounds selected for further analysis to predict the ADME/T parameter, such as, predict physicochemical descriptors, drug likeliness, and toxicity. Two servers had used to calculate the important information required to validate the selected bioactive ligands. The results achieved from the two servers listed in Table 4.

According to the results, GI absorption of all molecules was high. TPSA is an important interpreter for BBB penetration. The standard acceptable range of TPSA is from 90 to 140. If the TPSA value is less than 90 then it has the possibility to cross BBB. Boiled egg from SwissADME for all the molecules had analyzed. The boiled egg rendered according to WLOGP vs TPSA. This graphical representation illustrated that molecules, which presented in the yellow portion,

Table 1 Consensus binding affinities of 22 bioactive molecules with ABL1

ABL1				
PubChem ID	AutoDock affinity (kcal/mol)	Chimera affinity (kcal/mol)	Achilles affinity (kcal/mol)	Mcule affinity (kcal/mol)
4369496	−9.8	−10.3	−11.1	−8.6
25128185	−9.2	−9.7	−11.2	−8.9
24848331	−9.5	−9.4	−11.2	−8.9
24971209	−9.6	−9.7	−10.8	−8
10110378	−9.4	−10.4	−11.3	−8.7
73353596	−10.1	−9.7	−11.3	−9.6
2931814	−9.3	−9.3	−11.3	−8.3
72724706	−9.8	−10.5	−10.6	−7.4
10181160	−10.9	−10.6	−11.8	−8.3
25125902	−9.2	−9.3	−10.8	−9.7
51351018	−10.2	−10.4	−11.2	−8.6
25125572	−10.5	−10.7	−11.2	−9
46231494	−10.1	−10.1	−10.8	−8.9
9822042	−8.4	−9.8	−10.2	−8.5
10111108	−9.1	−10	−10.4	−8.4
10181075	−8.7	−9.4	−10.3	−8.5
24970384	−9.8	−8.6	−9	−8.8
25235817	−9.4	−8.6	−9.6	−8.5
44273619	−8.6	−8.7	−8.6	−8.9
44340691	−8.8	−9.6	−10	−7.6
51351016	−8.6	−8.5	−10.1	−8.5
58172700	−10.6	−9.3	−10.2	−9.2

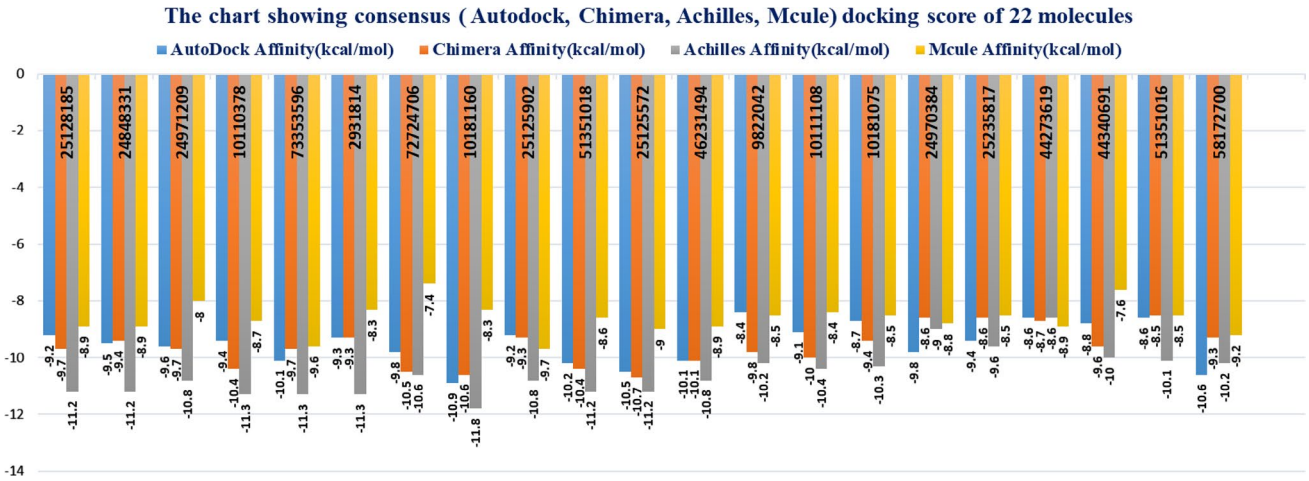

Fig. 2 The chart showing consensus (Autodock, Chimera, Achilles, Mcule) docking score of 22 molecules

Table 2 molecules under Lipinski's rule (A) and molecules under Veber filter (B)

A					B			
Lipinski's rule					Veber filter			
S/N	Title	MW	HBA	HBD	S/N	Title	nRB	TPSA
1	2931814	423.21	6	0	1	2931814	5	60.63
2	4369496	479.24	8	2	2	4369496	8	84.69
3	9822042	395.17	6	2	3	9822042	6	78.21
4	10110378	381.16	6	2	4	10110378	6	78.21
5	10111108	392.14	7	2	5	10111108	6	102
6	10181075	429.14	6	2	6	10181075	7	78.21
7	10181160	431.17	6	2	7	10181160	6	78.21
8	24848331	494.27	7	3	8	24848331	8	85.89
9	24970384	481.26	8	3	9	24970384	8	84.36
10	24971209	467.24	8	3	10	24971209	8	84.36
11	25125572	464.2	8	3	11	25125572	9	107.31
12	25125902	486.16	8	3	12	25125902	9	107.31
13	25128185	518.17	8	3	13	25128185	10	107.31
14	25235817	493.26	8	2	14	25235817	8	84.69
15	44273619	485.19	7	1	15	44273619	8	86.49
16	44340691	382.15	7	3	16	44340691	6	104.23
17	46231494	478.25	7	1	17	46231494	8	72.66
18	51351016	410.19	7	3	18	51351016	7	104.23
19	51351018	478.21	8	3	19	51351018	10	107.31
20	58172700	475.21	8	2	20	58172700	7	93.81
21	72724706	409.19	6	2	21	72724706	6	78.21
22	73353596	472.2	7	3	22	73353596	8	104.23

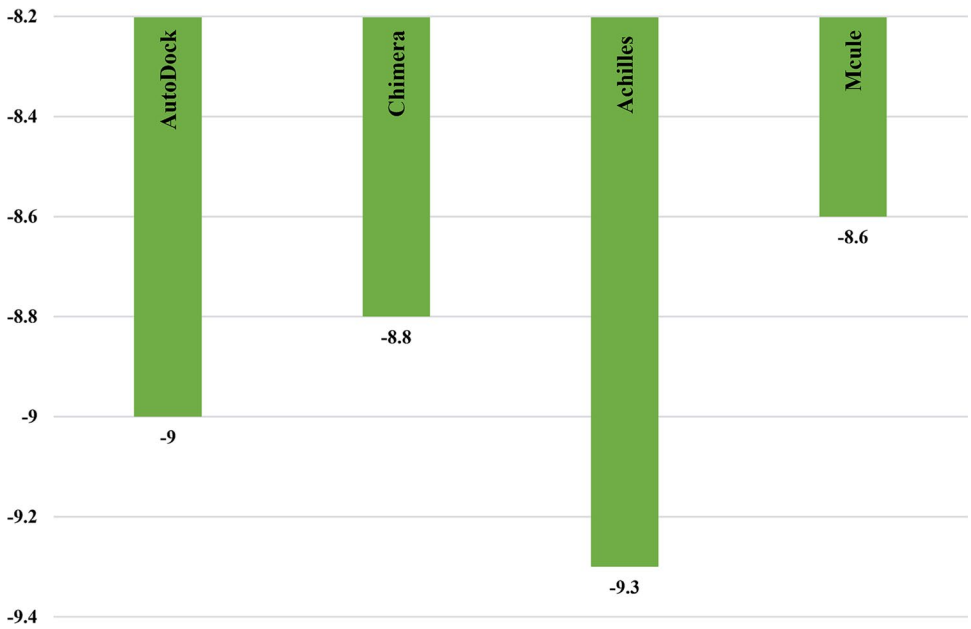

Fig. 3 Consensus (Autodock, Chimera, Achilles, Mcule) docking score of Imatinib

Table 3 Residual interaction results of ABL1 with 22 bioactive molecules

S/N	PubChem code	Interacting residues	Distance	Co-ordinates	Other weak residual Interactions
1	4369496	H bond: ARG A:386 TYR A:393 C–H bond: ALA A:397	2.18 Å 2.74 Å 1.96 Å 3.54 Å	12.4108, 137.806, 31.0749	Pi-Alkyl: LEU B:376, HIS A:396; Van Der Waals: PHE A:359, LEU A:384, ARG A:362, SER A:385, MET A:388, TYR B:342, ASN B:374 GLU B:373, GLY B:372, THR B: 319, PHE B:317, LEU B:266, THR B:267
2	10181160	H bond: ASP A:381 PHE A:382 C–H bond: LEU A:384	2.23 Å 2.54 Å 3.58 Å	22.0183, 129.415, 24.6427	Pi Sigma: LEU A:384; Pi Pi T Shaped: PHE A:359, TYR A:253; Alkyl: LEU A:301; Pi Alkyl: VAL A:256, ALA A:269, LYS A:271, LEU A:370, ILE A:301, ARG A:386, ALA A:380; Van Der Waals: GLY A:383, SER A:385, THR A:315, VAL A:299, GLU A:292, ILE A:293
3	25125572	H Bond: ASP A:381 PHE A:382	2.49 Å 2.29 Å	22.3764, 129.193, 24.1285	Pi Pi T Shaped: PHE A:359, PHE A:282; Alkyl: LEU A:301; Pi Alkyl: ILE A:313, ARG A:386, LYS A:271, VAL A:299, ALA A:380, LEU A:384; Van Der Waals: ILE A:293, GLU A:292, SER A:385, GLY A:383, THR A:315, LEU A:370, TYR A:253, GLY A:321, ALA A:269, VAL A:256
4	46231494	C–H Bond: THR A:306	3.53 Å	24.432, 133.221, 20.6791	Pi Sigma: THR A:315, ASP A:381; Pi Pi Stacked: PHE A:382; Pi Alkyl: LEU A:370, ALA A:380, LEU A:301, ILE A:313, LYS A:271; Van Der Waals: VAL A:299, TYR A:253, ASN A:368, LYS A:305, PRO A:309
5	51351018	H Bond: TYR B:253 MET B:318 C–H Bond: THR B:272	2.3 Å 2.75 Å 3.77 Å	11.3954, 159.638, 38.4229	Pi Pi Stacked: PHE B:382; Alkyl: LEU B:248; Pi Alkyl: VAL B:256, ALA B:380, LYS B:271, TYR B:253; Van Der Waals: GLY B:321, PHE B:317, GLU B:316, ALA B:269, LEU B:370, GLU B:255, PHE B:283, GLY B:254, ASN B:368
6	58172700	H Bond: MET B:318	2.23 Å	11.6348, 159.739, 37.1487	Pi Sigma: LEU B:248, LEU B:370; Pi Pi Stacked: PHE B:382, PHE B:317; Pi Pi T Shaped: TYR B:253; Alkyl: LEU B:370, ALA B:380; Pi Alkyl: ALA B:380, ALA B:269, VAL B:256, LYS B:271, TYR B:253, PHE B:283; Van Der Waals: GLU B:286, GLY B:321, GLU B:316, THR B:315, GLU B:255, GLY B:254, ASN B:368
7	72724706	_	_	22.8233, 129.394, 23.1002	Pi Sigma: ILE A:313, PHE A:382; Alkyl: LYS A:271, ALA A:269, VAL A:256, ALA A:380; Pi Alkyl: LEU A:384, LEU A:301, TYR A:253, LEU A:370, LYS A:271, ALA A:269, VAL A:256; Van Der Waals: PHE A:359, ILE A:293, SER A:385, ASP A:381, VAL A:299, THR A:315
8	73353596	H Bond: PHE A:382 ASP A:381 VAL A:299	2.27 Å 2.76 Å 2.38 Å	24.9059, 127.344, 19.6449	Pi Sigma: LEU A:248, LEU A:301; Pi Pi Stacked: PHE A:317; Pi Alkyl: VAL A:256, ALA A:269, LEU A:370, LYS A:271, ALA A:380, ILE A:313; Van Der Waals: THR A:319, GLY A:249, GLY A:321, MET A:318, TYR A:253, THR A:315, GLN A:300, GLU A:292

Table 3 (continued)

S/N	PubChem code	Interacting residues	Distance	Co-ordinates	Other weak residual Interactions
9	2931814	H Bond: TYR B:342 LYS B:378 C–H Bond: PRO B:296	2.84 Å 2.76 Å 2.60 Å 3.39 Å	16.6548, 138.949, 34.596	Pi Sigma: LEU B:376, PRO B:296; Amide Pi Stacked: HIS B:295; Pi Pi T Shaped: TYR B:342; Alkyl: PRO B:296; Pi Alkyl: MET A:388; Van Der Waals: GLU B:373, ASN B:374, TYR A:393, GLN B:300, LYS B:294, GLN B:346, HIS B:490, ASN B:297, SER B:349, THR B:345
10	9822042	H Bond: MET A:318	2.04 Å	23.8282, 130.107, 18.6372	Pi Sigma: ALA A:269, LEU A:370, PHE A:382, ILE A:313; Pi Pi Stacked: PHE A:382; Pi Pi T Shaped: TYR A:253; Alkyl: VAL A:299; Pi Alkyl: VAL A:256, ALA A:380, LYS A:271; Van Der Waals: LEU A:248, GLY A:254, PHE A:317, GLU A:316, THR A:315, ASP A:381
11	10110378	C–H Bond: VAL A:299	3.51 Å	24.5197, 127.861, 19.1718	Pi Sigma: ASP A:381, THR A:315; Pi Pi Stacked: PHE A:317; Pi Pi T Shaped: TYR A:253; Alkyl: LEU A:248; Pi Alkyl: ILE A:313, LEU A:301, ALA A:380, LYS A:271, LEU A:370, VAL A:256, ALA A:269; PHE A:382, MET A:318, GLY A:321
12	10111108	H Bond: ASP A:381 PHE A:382	2.19 Å 2.09 Å	21.8154, 130.092, 24.3853	Pi Alkyl: LEU A:384, ALA A:380, VAL A:299, LYS A:271, LEU A:301, ILE A:313; Van Der Waals: TYR A:253, LEU A:370, VAL A:256, ALA A:269, THR A:315, PHE A:359, ARG A:386, SER A:385
13	10181075	H Bond: ASP A:381 PHE A:382	2.81 Å 2.18 Å	21.6552, 130.108, 24.4275	Pi Sigma: LEU A:301, TYR A:253; Pi Pi T Shaped: PHE A:382; Alkyl: ALA A:269; Pi Alkyl: LYS A:271, VAL A:299, ALA A:380, ILE A:313; Van Der Waals: GLY A:383, LEU A:384, SER A:385, ARG A:386, LEU A:370, PHE A:359, ARG A:362, VAL A:256, THR A:315
14	24848331	H Bond: TYR B:342 TYR A:393 PHE B:317 C–H Bond: GLU B:316	2.43 Å 1.95 Å 1.86 Å 3.45 Å	13.1905, 139.735, 33.2445	Pi Donor H Bond: ASN B:297 (2.81Å), GLU B:373 (2.75Å); Alkyl: MET A:388; Pi Alkyl: LEU B:376; Van Der Waals: SER B:349, HIS B:490, THR B:345, GLN B:346, PRO B:296, ARG A:386, ASN B:374, HIS A:396, GLY B:372, THR B:319, MET B:318, LEU B:266
15	24970384	C–H Bond: TYR A:320	3.52 Å	24.807, 126.103, 13.0557	Pi Sigma: LEU A:348, LEU A:370; Pi Pi Stacked: TYR A:253, PHE A:382; Pi Alkyl: LYS A:271, ALA A:380, ALA A:269, VAL A:256; Van Der Waals: ASN A:368, ILE A:313, THR A:315, MET A:318, GLY A:321, PHE A:317, GLU A:329, GLY A:254, GLY A:249, THR A:319
16	24971209	H Bond: GLU B:329 C–H Bond: MET B:318	3.05 Å 3.27 Å 3.48 Å	0.945508, 147.724, 35.9714	Pi Sigma: LEU B:248; Pi Pi Stacked: PHE B:317; Pi Pi T Shaped: TYR B:253, TYR B:320; Pi Alkyl: ALA B:269, LEU B:320, TYR B:320, LEU B:248; Van Der Waals: GLY B:321, ASN B:322, GLY B:249, GLN B:252, ASP B:325, TYR B:326, CYS B:330, GLU B:334, ASN B:331

Table 3 (continued)

S/N	PubChem code	Interacting residues	Distance	Co-ordinates	Other weak residual Interactions
17	25125902	H Bond: ASPA:381 PHE A:382 ARG A:386	2.73 Å 2.28 Å 2.08 Å	19.1007, 131.285, 28.5898	Alkyl: ARG A:386; Pi Alkyl: MET A:388, LEU A:301, PHE A:359; Van Der Waals: GLU A:292, TYR A:393, TYR B:342, SER A:385, LEU A:384, ALA A:380, ILE A:313, LYS A:271
18	25128185	H Bond: PHE A:382 ASP A:381 ARG A:386 C–H Bond: LEU A:384	2.55 Å 2.22 Å 2.53 Å 2.53 Å	22.1084, 129.295, 23.8136	Pi Pi T Shaped: PHE A:359, PHE A:382; Alkyl: LYS A:271; Pi Alkyl: VAL A:299, ILE A:313, ALA A:380, ARG:386, TYR A:253; Van Der Waals: LEU A:370, VAL A:256, ALA A:269, THR A:315, LEU A:301, GLY A:383, SER A:385, GLU A:292, ILE A:293
19	25235817	H Bond: ARG A:386 C–H Bond: SER A:385	2.47 Å 3.38 Å	22.5461, 129.631, 23.8361	Pi Sigma: LEU A:301; Pi Pi Stacked: PHE A:382; Alkyl: LEU A:301, LEU A:370, VAL A:256, LYS A:271; Pi Alkyl: LEU A:384, ILE A:313, ALA A:380, TYR A:253; Van Der Waals: PHE A:359, ILE A:293, GLU A:292, VAL A:304, ASP A:381, VAL A:299, THR A:315, ALA A:269
20	44273619	C–H bond: ASP A:381 PHE A:382	3.32 Å 3.54 Å	22.2102, 129.833, 22.8799	Pi Sigma: THR A:315; Pi Pi T Stacked: TYR A:253; Alkyl: ILE A:313; Pi Alkyl: ALA A:380, ALA A:269, VAL A:299, LYS A:271, LEU A:384, ILE A:313; Van Der Waals: ASN A:368, GLY A:383, ILE A:293, PHE A:359, GLU A:292, LEU A:301, VAL A:256, LEU A:370
21	44340691	H bond: MET B:318 THR B:272	2.23 Å 1.91 Å	11.7928, 158.454, 36.3231	Pi Sigma: LEU B:370, LEU B:248; Pi Pi Stacked: PHE B:317, PHE B:382; Pi Pi T Shaped: TYR B:253; Pi Alkyl: VAL B:299, VAL B:256, ALA B:380, LEU B:370, ALA B:269, LYS B:271; Van Der Waals: GLU B:255, PHE B:283, LEU B:273, GLY B:254, GLY B:321, THR B:315
22	51351016	H bond: MET A:318	2.96 Å	23.499, 130.108, 18.5412	Pi Donor H bond: GLY A:254 (3.24Å); Pi Sigma: ILE A:313, PHE A:382, LEU A:370; Pi–Pi T Shaped: TYR A:253; Pi–Pi Stacked: PHE A:382; Pi Alkyl: ALA A:269, VAL A:256, LYS A: 271, ILE A:313, PHE A:382; Van Der Waals: GLY A:321, PHE A:317, LEU A:248, VAL A:299, THR A:315, ALA A:380, ASP A:381

literally can penetrate the blood–brain barrier (BBB). Red and blue colored dots (molecules) indicated PGP positive or PGP negative. Blue colored molecules have the possibility to efflux by PGP positive and red-colored molecules cannot efflux. According to TPSA score from Boiled egg analysis, PCID 9822042, PCID 10110378, PCID 10181075, PCID 24970384, PCID 25235817, PCID 44273619, PCID 2931814 and PCID 46291494 molecules were BBB permeate positive and dropped out. Based on ESOL LogS scale all molecules were within − 4.2 to − 5.97, which exhibited normal water solubility. All molecules were within range (from − 0.4 to 5.6) of MLogP except PCID 24848331, which showed − 1.53. Log Kp (the skin permeability coefficient) of all molecules were ranging from − 5.3 cm/s to − 7.02 cm/s.

Table 4 ADMET profile of 22 bioactive molecules

Molecule	TPSA	GI absorption	BBB permeant	Pgp substrate	CYP2D6 inhibitor	log Kp (cm/s)	Synthetic accessibility	AMES toxicity	Carcinogens	Acute oral toxicity
2931814	62.22	High	Yes	Yes	Yes	−5.82	3.09	NT	NC	III
4369496	86.28	High	No	Yes	Yes	−6.99	3.64	NT	NC	III
9822042	79.8	High	No	Yes	Yes	−5.71	3.14	NT	NC	III
10110378	79.8	High	No	Yes	Yes	−5.88	3	NT	NC	III
10111108	103.59	High	No	Yes	Yes	−6.41	3.01	NT	NC	III
10181075	79.8	High	No	Yes	Yes	−5.9	3.17	NT	NC	III
10181160	79.8	High	No	No	Yes	−5.3	3.25	NT	NC	III
24848331	87.48	High	No	Yes	No	−6.82	3.82	NT	NC	III
24970384	89.18	High	No	Yes	Yes	−6.84	3.62	NT	NC	III
24971209	89.18	High	No	Yes	Yes	−7.02	3.66	NT	NC	III
25125572	108.9	High	No	No	Yes	−6.27	3.52	Toxic	Carcinogens	III
25125902	108.9	High	No	Yes	Yes	−6.38	3.88	Toxic	Carcinogens	III
25128185	108.9	High	No	Yes	Yes	−6.38	3.88	Toxic	Carcinogens	III
25235817	86.28	High	No	Yes	Yes	−6.81	3.78	NT	NC	III
44273619	86.28	High	No	Yes	Yes	−6.81	3.78	NT	NC	III
44340691	105.82	High	No	Yes	Yes	−6.63	2.96	NT	NC	II
46231494	74.25	High	Yes	Yes	Yes	−6.29	3.96	NT	NC	III
51351016	105.82	High	No	Yes	Yes	−6.87	3.21	NT	NC	II
51351018	108.9	High	No	No	Yes	−6.51	3.61	NT	NC	II
58172700	97.62	High	No	Yes	Yes	−6.09	3.75	NT	NC	III
72724706	79.8	High	No	Yes	Yes	−5.53	3.19	NT	NC	III
73353596	105.82	High	No	No	Yes	−6.07	3.32	NT	NC	II
Imatinib	86.28	High	No	Yes	Yes	−6.81	3.78	NT	NC	III

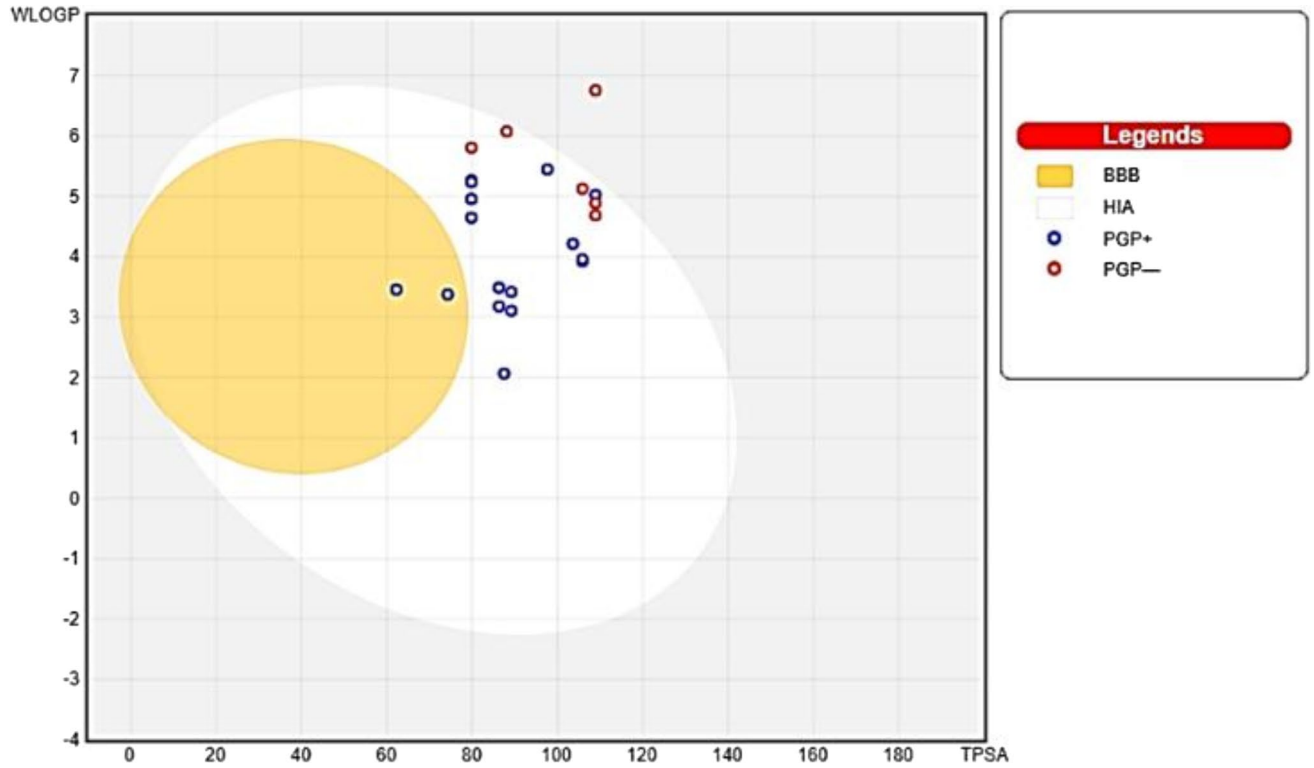

Fig. 4 Boiled egg analysis from SwissADME for 22 bioactive molecules

The more negative the log kp, the less skin permeate was the molecule. Based on Log Kp, PCID 24971209 dropped out. According to a carcinogen and AMES toxicity profile, PCID 25128185, PCID 10111108, PCID 25125572 and PCID 25125902 molecules showed positive toxicity signs and dropped out.

According to acute oral toxicity (Level I Fatal if swallowed, Level II Fatal if swallowed, Level III Toxic if swallowed, Level IV Harmful if swallowed, Level V may be Harmful if swallowed), PCID 44340691, PCID 51351016, PCID 51351018 and PCID 73353596 were dropped out as they had shown Level II toxicity.

According to the synthetic accessibility profile (SA score 1 means very easy to synthesize and 10 means very difficult to synthesize), PGP Substrate profile, and TPSA value from boiled egg analysis and considering other parameters, PCID 4369496, PCID 10181160, PCID 58172700 and PCID 72724706 had fulfilled all of the requirements of ADMET. The ADMET data (Boiled egg analysis from SwissADME) of 22 molecules presented in Fig. 4 and the structure of the selected four molecules showed in Fig. 5.

Multi-target analysis

Though ABL1 is the key target for CML, there are other proteins CSF1R, KIT, LCK, ABL2, PDGFRA, and PDGFRB, which could be also important target to combat CML. After ADMET analysis, PCID 72724706, PCID 10181160, PCID 4369496 and PCID 58172700 bioactive molecules found as potential hit molecules. Consensus docking scores of imatinib and hits with the CSF1R, KIT, LCK, ABL2, PDGFRA, and PDGFRB illustrated in Figs. 6 and 3D & 2D interaction of selected four molecules with ABL1 presented in Fig. 7.

Molecular dynamics simulation study

The protein ABL1 is an important drug target in the treatment of CML. To account for the flexibility of the protein and selected four ligands, a 50 ns molecular dynamics simulation of the docked complexes carried out. Four main parameters analyzed throughout the simulations, which

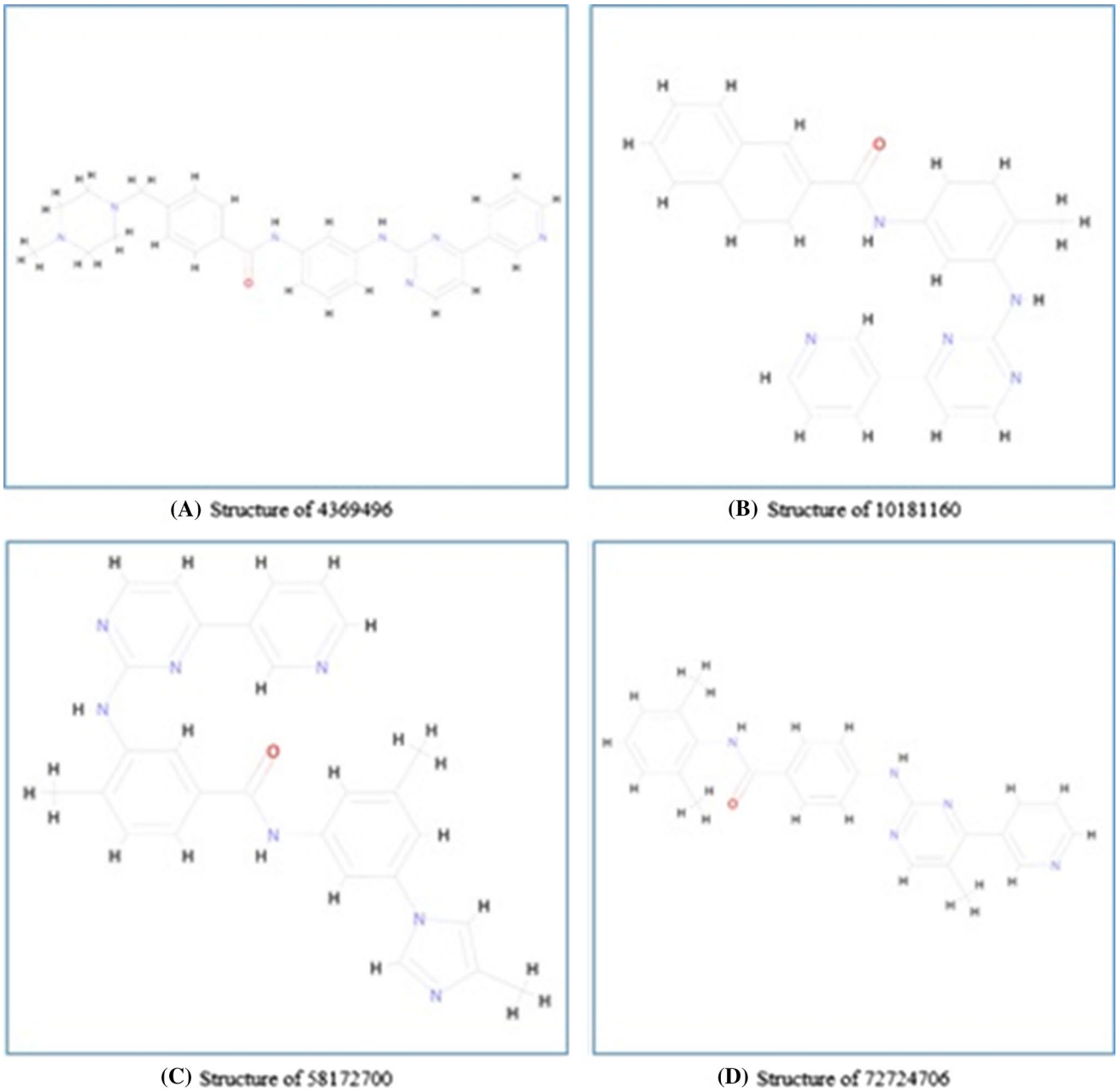

Fig. 5 Structures of desired four molecules (**a**) PCID 4369496, **b** 10181160, **c** PCID 58172700 and **d** PCID 72724706

were Root Mean Square Deviation (RMSD) and Root Mean Square Fluctuations (RMSF), Radius of gyration of the complexes.

Root mean square deviation (RMSD)

The stability of the complexes found validated by calculating the root mean square deviation. The RMSD value showed in Fig. 8 and in which observed range up to 6.5 Å showing that the systems are well converged. —PCID 4369496 was stable up to 34 ns then deviated. PCID 10181160 became stable after 23 ns, PCID 58172700 remained stable from 8 ns to 43 ns then deviation occurred. PCID 72724706 stabilized after 33 ns. PCID 10181160 and PCID 72724706 showed greater stability than the rest two.

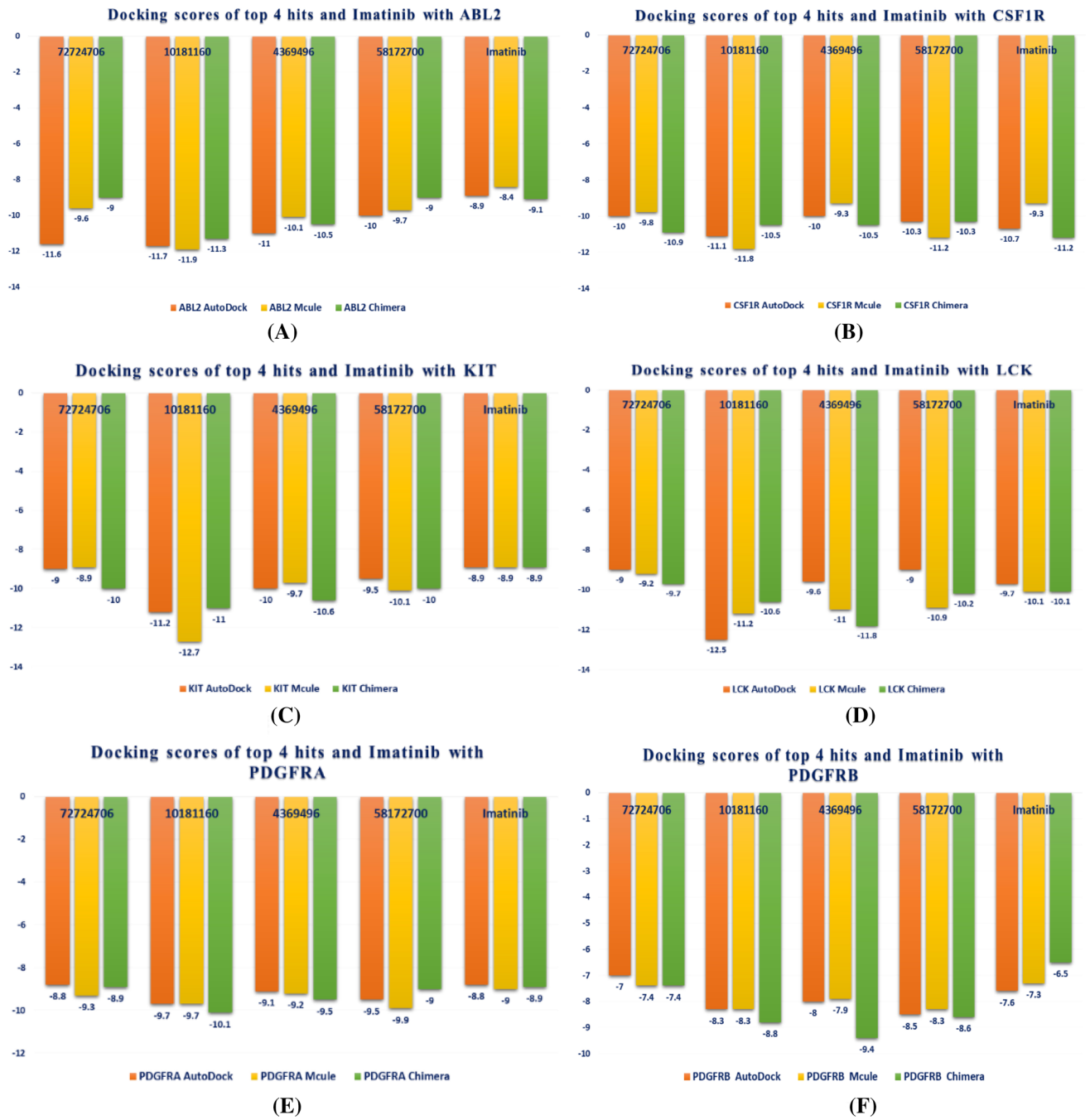

Fig. 6 Consensus docking scores of top 4 bioactive molecules and imatinib with ABL2 (**a**), CSF1R (**b**), KIT (**c**), LCK (**d**), PDGFRA (**e**) and PDGFRB (**f**)

Root mean square fluctuation (RMSF)

The root mean square fluctuation evident in Fig. 9. On this plot, peaks demonstrate the areas of the protein that fluctuated most in the entire simulation period. The overall fluctuations of the RMSF of the ligands found from a range of 1–14 Å throughout the simulation. The average RMSF values for the generated molecules achieved 13.07 Å

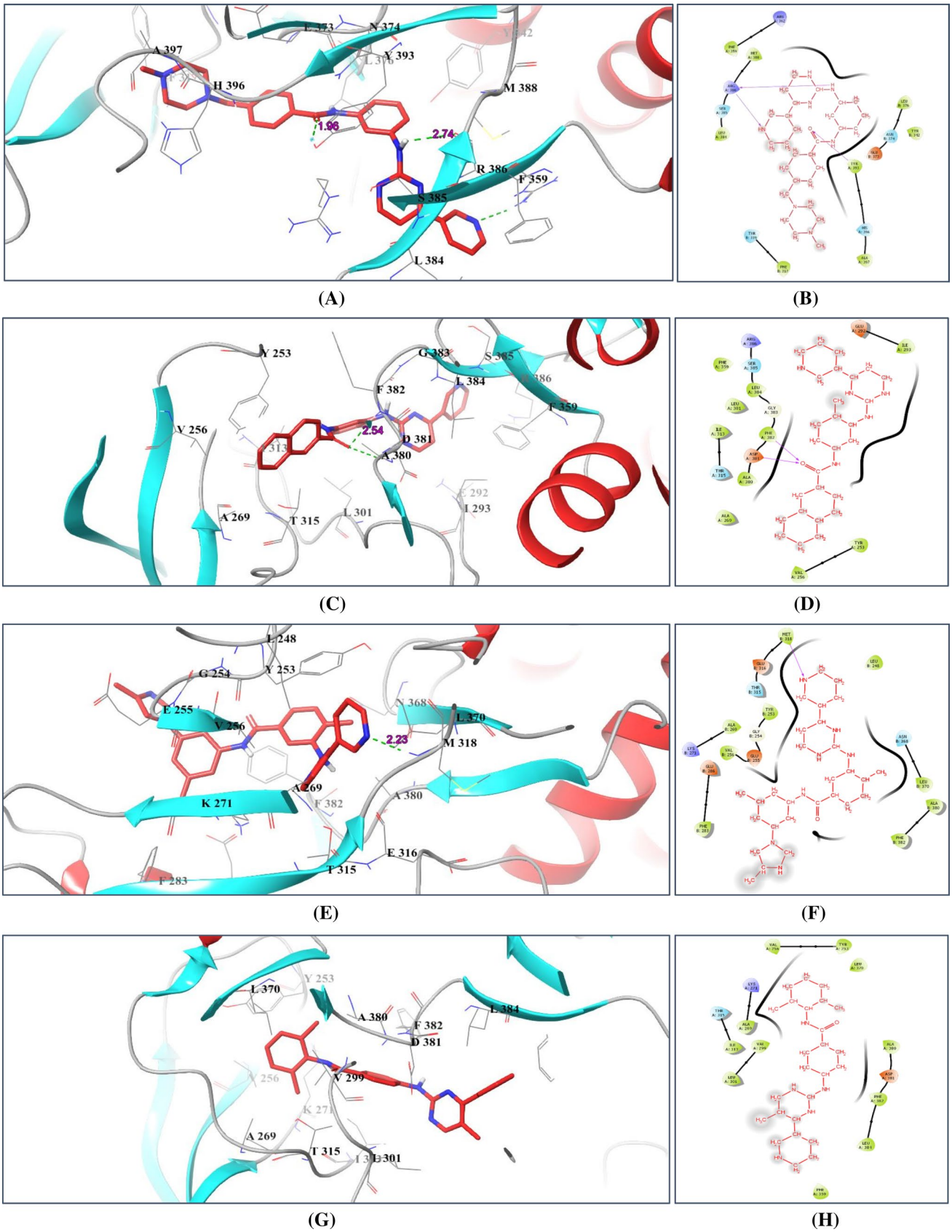

Fig. 7 3D and 2D interaction diagram of PCID 4369496 (**a**, **b**), PCID 10181160 (**c**, **d**), PCID 58172700 (**e**, **f**), PCID 72724706 (**g**, **h**) with ABL1

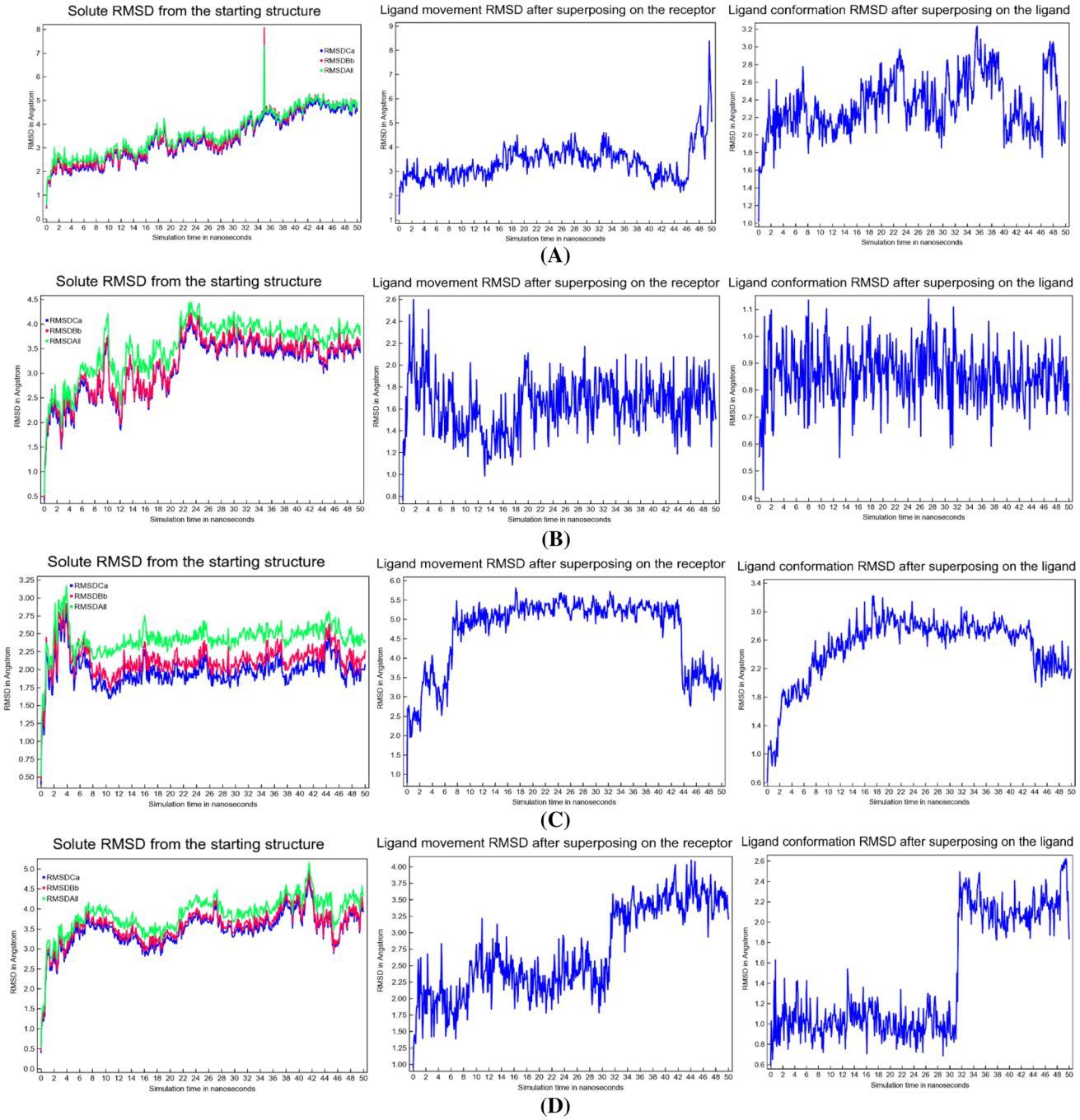

Fig. 8 RMSD of the ABL1 with ligand PCID 4369496 (**a**), PCID 10181160 (**b**), PCID 58172700 (**c**) and PCID 72724706 (**d**)

(PCID 4369496), 11.65 Å (PCID 10181160), 6.08 Å (PCID 58172700) and 5.78 Å (PCID 72724706) in which the protein flexibility had conferred.

The radius of gyration (R_g)

The radius of gyration shows the compactness of protein and protein–ligand complex i.e., how much protein is folded or

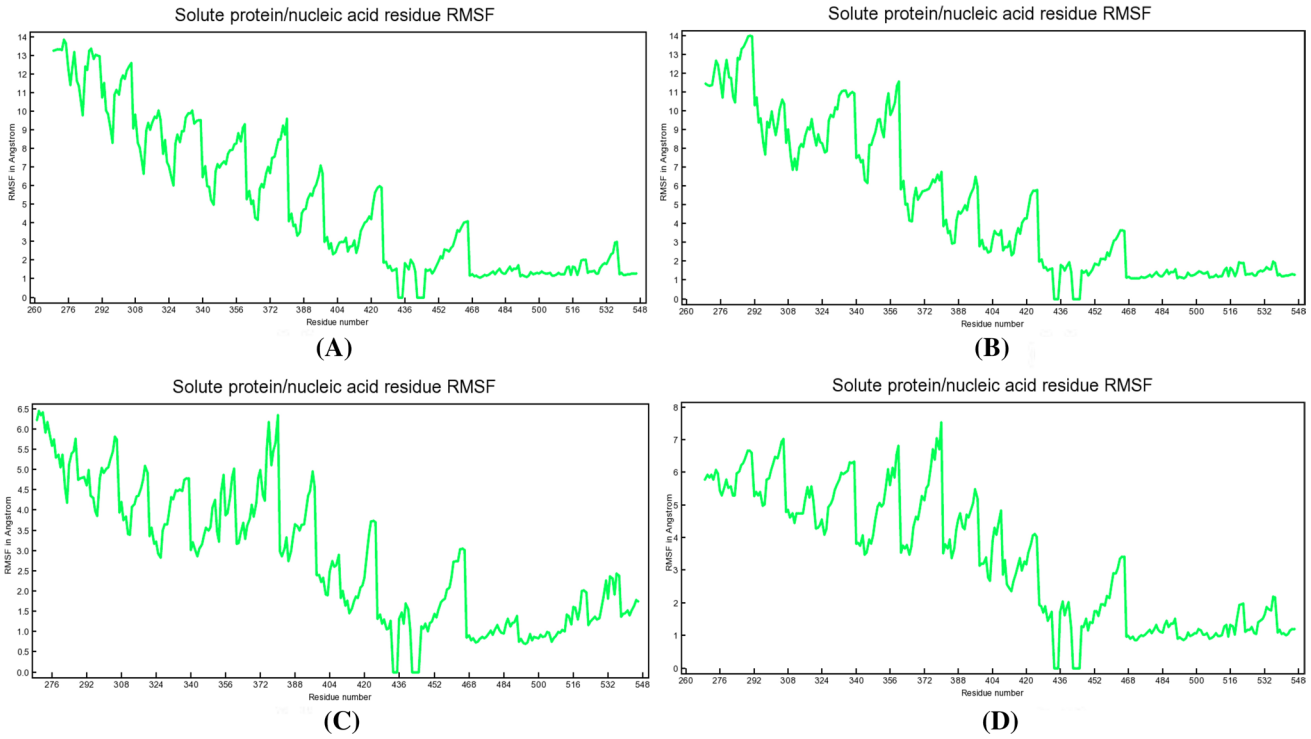

Fig. 9 RMSF data for each complex

unfolded with or without ligand. From Fig. 10, it had found that the radius of gyration of the molecules is constant over time and maintained the same mean value of 21.0 ± 0.5 Å. However, the oscillations were greater for PCID 4369496. R_g may suggest that this molecule was less stable than the rest. From the overall molecular dynamic study, these two compounds PCID 10181160 and PCID 72724706 formed stable complexes with ABL1 during 50-ns MD simulations.

Conclusion

The present, in silico studies, provides insight into the inhibition of ABL1, ABL2, CSF1R, KIT, LCK, PDGFRA, and PDGFRB by imatinib and its bioactive molecules. Virtual screening, Consensus docking studies, Multi-target analysis, and ADMET profiling suggest that PCID 4369496, PCID 10181160, PCID 58172700, and PCID 72724706, among 22 bioactive molecules from 135 bioactive molecules with the best docking scores than imatinib from a database of 1,77,000 molecules, are the most active inhibitors. These four molecules further selected for molecular dynamics (MD) simulation analysis, which revealed that the two compounds PCID 10181160 and PCID 72724706 formed stable complexes with ABL1 during 50-ns MD simulations. These lead molecules are the potential CML inhibitors that could resolve the resistance pattern. Further chemical synthesis, wet lab analysis, and experimental validation deserve the utmost attention.

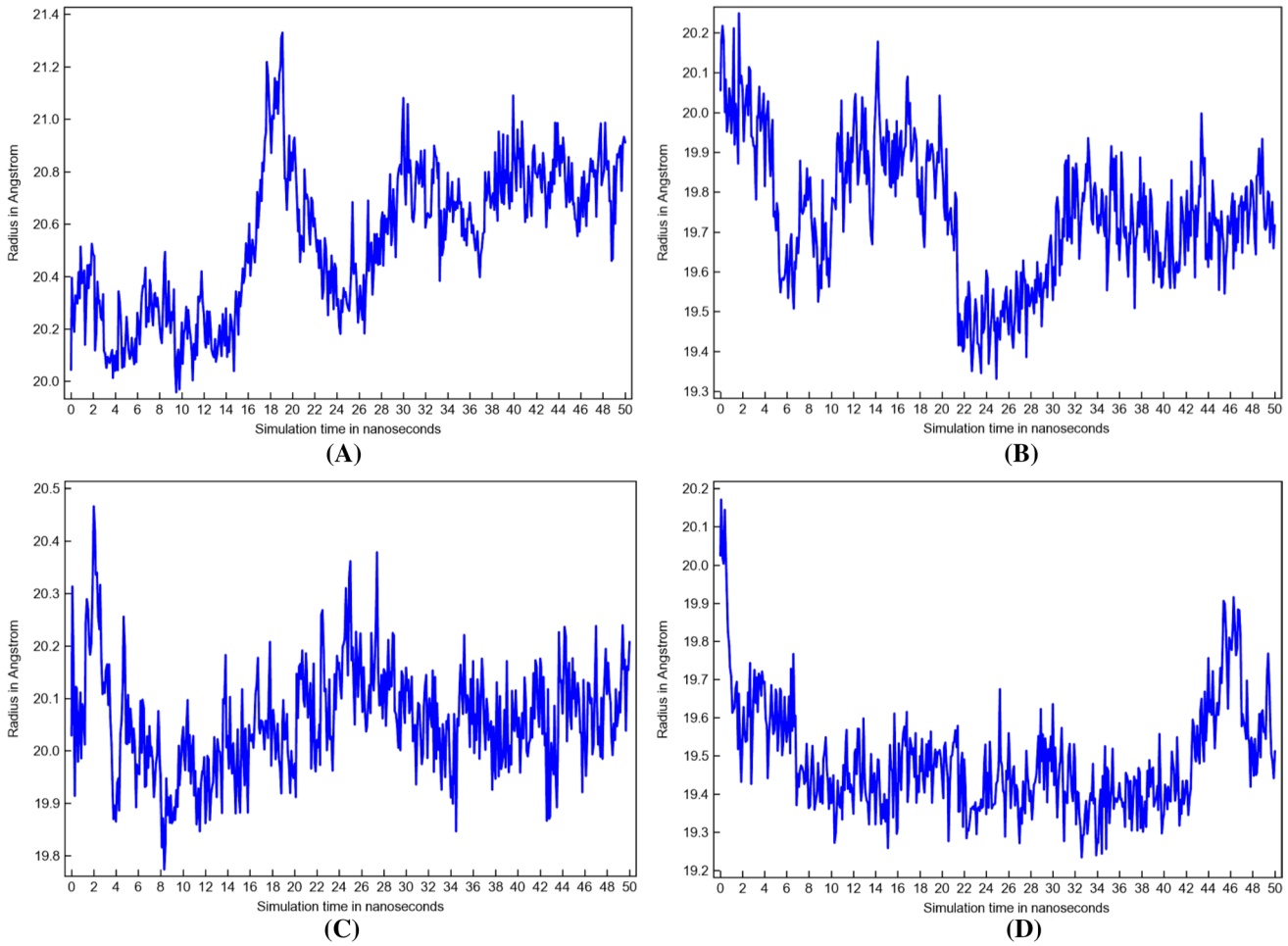

Fig. 10 Radius of gyration of ABL1 with four selected molecules

Acknowledgements Support to CBRL from Achilles blind docking server, OpenEye Scientific Software Inc. (Santa Fe, NM, USA) gratefully acknowledged. The research work had planned and conducted by AR, NHN & SCR. NQ and RM approved the research workflow, and proofread the article.

Funding This research did not receive any specific grant from funding agencies in the public, commercial, or not-for-profit sectors.

Data availability The experimental data used to support the findings of this study are included in the article.

Compliance with ethical standards

Ethical statement This article does not contain any studies with human participants or animals performed by any of the authors.

Conflict of interest Arifur Rahman has no conflict of interest. Nazmul Hasan Naheed has no conflict of interest. Sabreena Chowdhury Raka has no conflict of interest. Nazmul Qais has no conflict of interest. A. Z. M. Ruhul Momen has no conflict of interest.

References

Dickson CJ, Madej BD, Skjevik ÅA, Betz RM, Teigen K, Gould IR, Walker RC (2014) Lipid14: the amber lipid force field. J Chem Theory Comput 10(2):865–879

Druker BJ, Sawyers CL, Kantarjian H, Resta DJ, Reese SF, Ford JM, Talpaz M (2001) The activity of a specific inhibitor of the BCR–ABL tyrosine kinase in the blast crisis of chronic myeloid leukemia and acute lymphoblastic leukemia with the Philadelphia chromosome. N Engl J Med 344(14):1038–1042

Dundas J, Ouyang Z, Tseng J, Binkowski A, Turpaz Y, Liang J (2006) CASTp: computed atlas of surface topography of proteins with structural and topographical mapping of functionally annotated residues. Nucleic Acids Res 34(2):116–118

Eadie LN, Dang P, Goyne JM, Hughes TP, White DL (2018) ABCC6 plays a significant role in the transport of nilotinib and dasatinib, and contributes to TKI resistance in vitro, in both cell lines and primary patient mononuclear cells. PLoS ONE 13(1):e0192180

Faderl S, Talpaz M, Estrov Z, O'Brien S, Kurzrock R, Kantarjian HM (1999) The biology of chronic myeloid leukemia. N Engl J Med 341(3):164–172

Goldman JM, Melo JV (2003) Chronic myeloid leukemia—advances in biology and new approaches to treatment. N Engl J Med 349(15):1451–1464

Hassan NM, Alhossary AA, Mu Y, Kwoh CK (2017) Protein–ligand blind docking using QuickVina-W with inter-process spatio-temporal integration. Sci Rep 7(1):15451

Huang B (2009) MetaPocket: a meta approach to improve protein–ligand binding site prediction. OMICS 13(4):325–330

Isa MA, Majumdhar RS, Haider S (2018) In silico docking and molecular dynamics simulation of 3-dehydroquinate synthase (DHQS) from *Mycobacterium tuberculosis*. J Mol Model 24(6):132

Jabbour E, Kantarjian H (2014) Chronic myeloid leukemia: 2014 update on diagnosis, monitoring, and management. Am J Hematol 89(5):547–556

Jakalian A, Jack DB, Bayly CI (2002) Fast, efficient generation of high-quality atomic charges. AM1-BCC model: II. Parameterization and validation. J Comput Chem 23(16):1623–1641

Kang ZJ, Liu YF, Xu LZ, Long ZJ, Huang D, Yang Y, Liu Q (2016) The Philadelphia chromosome in leukemogenesis. Chin J Cancer 35(1):48

Krieger E, Vriend G (2014) YASARA View—molecular graphics for all devices—from smartphones to workstations. Bioinformatics 30(20):2981–2982

Krieger E, Vriend G (2015) New ways to boost molecular dynamics simulations. J Comput Chem 36(13):996–1007

Krieger E, Koraimann G, Vriend G (2002) Increasing the precision of comparative models with YASARA NOVA—a self-parameterizing force field. Proteins Struct Funct Bioinform 47(3):393–402

Krieger E, Nielsen JE, Spronk CA, Vriend G (2006) Fast empirical pKa prediction by Ewald summation. J Mol Graph Model 25(4):481–486

Le Coutre P, Ottmann OG, Giles F, Kim DW, Cortes J, Gattermann N, Kuliczkowski K (2008) Nilotinib (formerly AMN107), a highly selective BCR–ABL tyrosine kinase inhibitor, is active in patients with imatinib-resistant or-intolerant accelerated-phase chronic myelogenous leukemia. Blood 111(4):1834–1839

Maier JA, Martinez C, Kasavajhala K, Wickstrom L, Hauser KE, Simmerling C (2015) ff14SB: improving the accuracy of protein side chain and backbone parameters from ff99SB. J Chem Theory Comput 11(8):3696–3713

Mandlik V, Singh S (2016) Molecular docking and molecular dynamics simulation study of inositol phosphorylceramide synthase–inhibitor complex in leishmaniasis: insight into the structure based drug design. F1000Research. https://doi.org/10.12688/f1000research.9151.2

Mauro MJ (2006) Defining and managing imatinib resistance. ASH Educ Program B 1:219–225

Meng XY, Zhang HX, Mezei M, Cui M (2011) Molecular docking: a powerful approach for structure-based drug discovery. Curr Comput Aided Drug Des 7(2):146–157

Mitra S, Dash R (2018) Structural dynamics and quantum mechanical aspects of shikonin derivatives as CREBBP bromodomain inhibitors. J Mol Graph Model 83:42–52

Morris GM, Goodsell DS, Huey R, Olson AJ (1996) Distributed automated docking of flexible ligands to proteins: parallel applications of AutoDock 2.4. J Comput Aided Mol Des 10(4):293–304

Nagasundaram N, Zhu H, Liu J, Karthick V, Chakraborty C, Chen L (2015) Analysing the effect of the mutation on protein function and discovering potential inhibitors of CDK4: molecular modeling and dynamics studies. PLoS ONE 10(8):e0133969

Pascoini AL, Federico LB, Arêas ALF, Verde BA, Freitas PG, Camps I (2018) In silico development of new acetylcholinesterase inhibitors. J Biomol Struct Dyn 1:15

Pettersen EF, Goddard TD, Huang CC, Couch GS, Greenblatt DM, Meng EC, Ferrin TE (2004) UCSF Chimera-a visualization system for exploratory research and analysis. J Comput Chem 25(13):1605–1612

Quintás-Cardama A, Kantarjian H, Cortes J (2007) Flying under the radar: the new wave of BCR–ABL inhibitors. Nat Rev Drug Discov 6(10):834

Rask-Andersen M, Zhang J, Fabbro D, Schiöth HB (2014) Advances in kinase targeting: current clinical use and clinical trials. Trends Pharmacol Sci 35(11):604–620

Sánchez-Linares I, Pérez-Sánchez H, Cecilia JM, García JM (2012) High-throughput parallel blind virtual screening using BINDSURF. BMC Bioinform 13(14):S13

Shah NP, Nicoll JM, Nagar B, Gorre ME, Paquette RL, Kuriyan J, Sawyers CL (2002) Multiple BCR–ABL kinase domain mutations confer polyclonal resistance to the tyrosine kinase inhibitor imatinib (STI571) in chronic phase and blast crisis chronic myeloid leukemia. Cancer Cell 2(2):117–125

Shah RR, Morganroth J, Shah DR (2013) Hepatotoxicity of tyrosine kinase inhibitors: clinical and regulatory perspectives. Drug Saf 36(7):491–503

Skelton AA, Fenter P, Kubicki JD, Wesolowski DJ, Cummings PT (2011) Simulations of the quartz (1011)/water interface: a comparison of classical force fields, ab initio molecular dynamics, and X-ray reflectivity experiments. J Phys Chem C 115(5):2076–2088

Steinberg M (2007) Dasatinib: a tyrosine kinase inhibitor for the treatment of chronic myelogenous leukemia and Philadelphia chromosome-positive acute lymphoblastic leukemia. Clin Ther 29(11):2289–2308

Stewart JJ (1990) MOPAC: a semiempirical molecular orbital program. J Comput Aided Mol Des 4(1):1–103

Szklarczyk D, Santos A, von Mering C, Jensen LJ, Bork P, Kuhn M (2015) STITCH 5: augmenting protein–chemical interaction networks with tissue and affinity data. Nucleic Acids Res 44(D1):D380–D384

Wang J, Wolf RM, Caldwell JW, Kollman PA, Case DA (2004) Development and testing of a general amber force field. J Comput Chem 25(9):1157–1174

Zoete V, Daina A, Bovigny C, Michielin O (2016) SwissSimilarity: a web tool for low to ultra-high throughput ligand-based virtual screening. J Chem Inf Model 56(8):1399–1404